Dynamic Modeling and Control Study of the NAO Biped Robot with Improved Trajectory Planning

Chapter · January 2012

DOI: 10.1007/978-3-642-22700-4_42

Dynamic Modeling and Control Study of the NAO Biped Robot with Improved Trajectory Planning

E. Hashemi and M. Ghaffari Jadidi

Abstract Motion study of bipedal robots necessitates correct solutions of the forward and inverse kinematics with optimized and fast closed form computations which justifies an accurate kinematic model. On the other hand, dynamic modeling and stability analysis are essential for control study of humanoid robots to reach robust walk. This chapter is focused on dynamic modeling of the Nao humanoid robot, made by Aldebaran Co., in the RoboCup standard platform league. Moreover, trajectory approximation with a cubic Spline and kinematic analysis are described in brief here in this chapter. Main constraints such as inertial forces and joint angles for the given position and nominal conditions are simulated, mathematically described, and verified through experimental results from the real robot sensory data. The above mentioned modifications on the solution together with the dedication of other physical properties in dynamic modeling results in more precise acceleration and torque values as it is concluded in this work.

Keywords Bipedal locomotion · Dynamic simulation · Inverse kinematics · Motion planning · Trajectory approximation

E. Hashemi (✉)
Faculty of Industrial and Mechanical Engineering,
Islamic Azad University, Qazvin Branch, Qazvin, Iran
e-mail: e.hashemi@qiau.ac.ir

M. Ghaffari Jadidi
Faculty of Electrical, Computer and IT Engineering,
Islamic Azad University, Qazvin Branch, Qazvin, Iran
e-mail: m.ghaffari@qiau.ac.ir

A. Öchsner et al. (eds.), *Materials with Complex Behaviour II*,
Advanced Structured Materials 16, DOI: 10.1007/978-3-642-22700-4_42,

1 Introduction

Bipedal locomotion has been a topic of great attention in a various researches performed on legged robots and is probably the most suitable method for robots to execute assigned maneuvers in a real environment with various obstacle conditions and geometry [1–3]. Extensive studies have been conducted on various control methods of bipedal walking and stability, and now biped robots are capable of walking with a certain amount of stability [4–9]. Combined Forward and Inverse Kinematics models are utilized to specify the reliable method to control motion and preserve stability as discussed in [10–12]. The humanoid bipedal locomotion needs reasonable solutions of the inverse kinematics and localization problems with optimized computations as illustrated in [13]. Since the end effector configurations and its exact locations are related to the above mentioned joint parameters with nonlinear characteristics, inverse kinematics problems are usually complicated. It is essential to do a transformation between the Cartesian end effector orientation and location vector and the corresponding vector of joint angular position which leads to determination of actuating signals and driver torque values in the dynamic model. Trajectory approximation, kinematic, and dynamic modeling are described in the following sections of this material.

2 NAO Walking Trajectory Generation

Kinematic and dynamic study of linkage systems are key and fundamental issues for trajectory control, motion planning and locomotion modeling which are discussed in [4, 5]. In order to attain a stable and reliable walk in different ground conditions such as regions containing obstacles, rough terrain and slopes, it is required to maintain the stability of the biped robot and adapt to such environmental conditions with a suitable foot motion and a smooth hip shift which justifies comprehensive study of trajectory generation and transformation to desirable joint angles and develop some specific controllers such as torque control methods.

Zero Moment Point (ZMP) stability criteria is introduced for the stability assessment of the bipedal robots during walking [14] and consideration of this criterion for trajectory generation has an essential role to reach a dependable trajectory for both foot and hip joints as studied in [15–17]. The presented method in [15] uses a stability margin to achieve a certain degree of stability instead of marginal stability. Walking cycles falls into two main stages including the single-support phase (SSP) and the double support phase (DSP). In the SSP, one foot is stationary on the ground and the other foot swings from the rear to the front, but both feet are in contact with the ground in DSP. DSP begins with the heel of the forward foot touching the ground, and ends with the toe of the rear foot taking off the ground [18]. The walking pattern can therefore be denoted uniquely by both foot and the hip trajectories as presented in [19, 20]. If foot and hip trajectories are

identified, all joint trajectories of the robot will be determined by the kinematic constraints and geometrical relations.

Trajectories considered for dynamic modeling are derived with the assumptions of 10 cm/s walking velocity and a 5 cm step length. Implementing velocity and kinematic constraints specified in Eq. A.1, Appendix brings about Eqs. 1 and 2 which comprehensively offered a cubic Spline for foot movement in *sagittal* plane in x and z directions.

$$x_f(t) = \begin{cases} -L_{step}, & t_1 < t < t_2 \\ -1.2848t^3 + 1.4202t^2 - 0.1938t - 0.0435, & t_2 < t < t_3 \\ -1.5144t^3 + 1.5855t^2 - 0.2334t - 0.0404, & t_3 < t < t_4 \\ L_{step}, & t_4 < t < T_{cycle} \end{cases} \tag{1}$$

$$z_f(t) = \begin{cases} FootHeight, & \\ -19.724t^3 + 10.2116t^2 - 1.2359t + 0.0412, & t_1 < t < t_2 \\ 8.1169t^3 - 9.8338t^2 + 3.575t - 0.3437, & t_2 < t < t_3 \\ FootHeight, & t_3 < t < t_4 \\ & t_4 < t < T_{cycle} \end{cases} \tag{2}$$

Torso trajectory with execution of the cubic Spline could be written as bellow in which coefficients are calculated by the method presented in [18–20] and mentioned in Eq. A.2, Appendix.

$$x_t(t) = \begin{cases} 1.4687t^3 - 0.1762t^2 + 0.0554t - 0.0228 & t_1 < t < t_2 \\ -0.3672t^3 + 0.3745t^2 + 0.0003t - 0.0209 & t_2 < t < t_4 \end{cases} \tag{3}$$

$$y_t(t) = \begin{cases} 1.3782t^3 - 0.0292t^2 - 0.239t, & t_1 < t < t_3 \\ -1.2079t^3 + 1.8328t^2 - 0.6859t + 0.0358, & t_3 < t < t_4 \\ -1.3768t^3 + 2.0862t^2 - 0.8126t + 0.0569, & t_4 < t < t_1 + T_{step} \\ 1.2066t^3 - 3.6491t^2 + 3.4353t - 0.9928, & t_1 + T_{step} < t < T_{cycle} \end{cases} \tag{4}$$

$$z_t(t) = \begin{cases} -0.8413t^3 + 0.2436t^2 + 0.0317t + 0.2 & t_1 < t < t_3 \\ 0.7766t^3 - 0.9214t^2 + 0.3113t + 0.1776 & t_3 < t < t_4 \end{cases} \tag{5}$$

Equations 3–5 are tailor made for a Nao robot's step length and velocity scenario and modified for the robot's torso within the above mentioned periods.

3 Kinematic and Dynamic Modeling

This section deals with the model derivation for Nao robot of the MRL team. The purpose of the model is to give the necessary insight of the system to design, test and simulate controllers for the above mentioned biped robot. The models

developed are a kinematic model to determine joint angles, link positions, velocities, and acceleration for different torso and foot trajectories and a dynamic model to estimate dynamic behavior of the links and related joint torques.

3.1 Inverse Kinematics

The kinematic model concerns relations between different joints on the robot and the position of the individual links. This is done by transforming from joint space to Cartesian space [21]. With this transformation, the position of the links' CoM is calculated from the given rotation of the joints. Required data for the forward kinematic model are the system phase and the angular position of the joints θ_n. Kinematic model output is the global position Gin the global Cartesian coordinates. Mechanical and geometrical data are already extracted from the Nao physical specifications provided by Aldebaran Co. and listed in Appendix. The calculated data for the link vectors are listed in Table 3 together with the accessible CoM vectors.

Denavit–Hartenberg (DH) method and an open loop serial chain system is used in [20–24] for determination of all the joint rotations. The first rotation is assumed in the supporting foot and the last rotation is considered in the non supporting foot. The frames are aligned with the global reference frame in case all the joints are in their zero state because no rotations are needed to describe the system when all the angles of the joints are zero. Furthermore, the position of the ground frame is fixed to the initial frame {0} such that the initial frames always contain the global position and all frames have the same direction when the angles are zero. As mentioned above, the kinematic model estimates the global velocity and acceleration vectors as explained in the following paragraphs. The global position of the links CoM, $\{G_n\}$ can be expressed as the following relation [23]:

$$\{G_n\} = \{G_{m,n-1}\} + {}^{0}_{n-1}R\{b_n\} \tag{6}$$

In which $\{b_n\}$ represents the CoM local position of link n. Position of joint $n-1$ in the global coordinates, $\{G_{m,n-1}\}$ is defined as:

$$\{G_{m,n-1}\} = {}^{0}_{n-2}R\{a_{n-1}\} + \{G_{m,n-2}\} \tag{7}$$

Local position vector of joints is shown by $\{a_i\}$ in Eq. 7. Controller design and development justifies making use of precise inverse kinematics and dynamic models to satisfy stability and agility requirements in biped robots such as Nao.

Nao robot has 21 degrees of freedom, including 6 in each leg introduced as ankle roll, ankle pitch, knee pitch, hip pitch, hip roll, and hip yaw-pitch. Yaw-pitch joints of the hips are physically bound and driven with one servo motor. The purpose of the inverse kinematic model is to determine the joint angles which yield a specific position of the limbs in Cartesian space. Inverse kinematics model

requires expected positions of links which could be attainable by torso and foot trajectories and calculates joint angles corresponding to the determined trajectories. Numerical and closed-form solutions are widely used to solve the inverse kinematics problems.

Goldenberg et al. [25] presented an iterative numerical solution to transform the desired position of a limb into joint angles by solving the pseudo inverse Jacobian to reach accurate results. One of the drawbacks of this method is this iterative method is a time consuming process for both legs solution and does not satisfy the time response requirements of the control loop model [22].

Closed-form solution of the non-linear equations of the robot manipulators with limited degrees of freedom is introduced as an alternative method of solving inverse kinematics equations. This method is also employed to carry out the solution of MRL team Nao robot's kinematic equations with utilization of Pieper's solution [23] for developing transformation and rotation matrices. This method and its modification is described in this section as an approach for solving related equations which enables the approach to compute the same hip Yaw-Pitch joint variable for both legs.

DH frame assignment and related coordinate sequences are shown in Fig. 1, and associated parameters are mentioned in Table 1. DH parameters for the right leg is assumed the same as the left one except α_6 which is $\pi/4$.

Homogeneous transformation ${}^{0}_{6}T$ which describes position and orientation of frame $\{6\}$ relative to frame $\{0\}$ is introduced as Eq. 8

$$ {}^{0}_{6}T = \begin{bmatrix} {}^{0}_{6}R & {}^{0}p_{6ORG} \\ 0 & 1 \end{bmatrix} \tag{8} $$

Position vector ${}^{0}p_{6ORG}$ expresses coordination of frame $\{6\}$ origin relative to frame $\{0\}$ in the homogeneous transformation matrix. Joint angles $\theta_1, \theta_2, \theta_3$ could also be computed by using ${}^{0}p_{6ORG}$, then the last three joint angles of each leg, $\theta_4, \theta_5, \theta_6$ are approximated using ${}^{0}_{6}R$ which is rotation matrix explaining orientation of frame $\{6\}$ relative to $\{0\}$. Since origins of frames $\{4\}$, $\{5\}$, $\{6\}$ are coincident at a point, ${}^{0}p_{6ORG}$ is equal to ${}^{0}p_{4ORG}$ and mathematically shown in Eq. 9. Calculation of ${}^{0}p_{6ORG}$ is vital because it results in determination of $\theta_1, \theta_2, \theta_3$ in Pieper's solution.

$$ \begin{aligned} {}^{0}p_{6ORG} = {}^{0}p_{4ORG} &= {}^{0}_{3}T \times^{3} p_{4ORG} = {}^{0}_{1}T \times {}^{1}_{2}T \times \begin{bmatrix} f_1(\theta_3) \\ f_2(\theta_3) \\ f_3(\theta_3) \\ 1 \end{bmatrix} \\ &= \begin{bmatrix} c_1 g_1(\theta_2, \theta_3) - s_1 g_2(\theta_2, \theta_3) \\ s_1 g_1(\theta_2, \theta_3) + c_1 g_2(\theta_2, \theta_3) \\ g_3(\theta_2, \theta_3) \\ 1 \end{bmatrix} = \begin{bmatrix} x \\ y \\ z \\ 1 \end{bmatrix} \end{aligned} \tag{9} $$

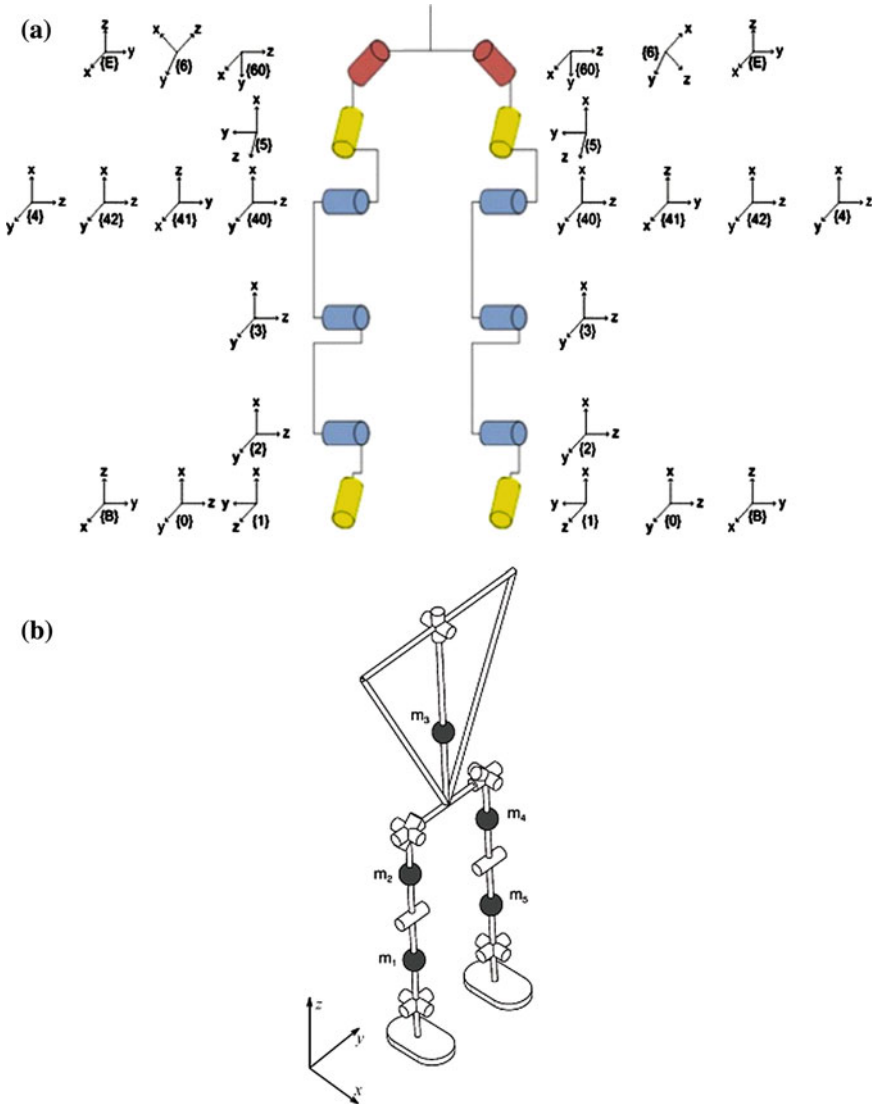

Fig. 1 **a** DH representation of legs for the Nao robot kinematic simulation; **b** mass and geometrical model for the Nao robot

In which c_1 and s_1 represent $Cos\,\theta_1$ and $Sin\,\theta_1$, and approximation functions f and g are given in the Appendix section of this chapter. The first three joint angles θ_1, θ_2 and θ_3 are estimated by position vector components x,y and z and solving Eqs. 10 and 11 simultaneously.

$$z = g_3(\theta_2, \theta_3) \tag{10}$$

Table 1 Dedicated DH parameter values for the left leg

Frame (joint)	α_i	a_i	d_i	θ_i
1	$-\pi/2$	0	0	θ_1
2	$\pi/2$	0	0	θ_2
3	0	Tibia length	0	θ_3
40	0	Thigh length	0	0
4	0	0	0	θ_4
5	$-\pi/2$	0	0	θ_5
6	$-\pi/4$	0	0	$\theta_6 - 3\pi/4$
41		$Rot_z(\pi/2) \times Rot_x(\pi/2)$		
42		$Rot_x(-\pi/2) \times Rot_z(-\pi/2)$		
60		$Rot_x(\pi/2) \times Rot_z(\pi/2)$		

$$r = x^2 + y^2 + z^2 = [g_1(\theta_2, \theta_3)]^2 + [g_2(\theta_2, \theta_3)]^2 + [g_3(\theta_2, \theta_3)]^2 \tag{11}$$

Variables a_1 and $s\alpha_1$ are influencing parameters in solution of Eqs. 10 and 11 and can be extracted from the geometric conditions of the left or right legs. The first joint angle θ_1 is estimated after analytic solution of the second and the third joint angles and replacing these two values in Eq. 9. The following paragraph presents calculation of θ_4, θ_5 and θ_6 in Pieper's solution using ${}^0_6R$ and the estimated first three joint angles. Computation of θ_1, θ_2 and θ_3 leads to calculation of ${}^0_3R$ using Eq. 12 which simply describes the relation between rotation matrices in frames {0}, {3} and {6}.

$${}^3_6R = \left({}^0_3R\right)^{-1} \times {}^0_6R \tag{12}$$

The cubic spline described in the previous section to generate trajectories for steady state walk is utilized to present the kinematic model. Validation of formulas for both left and right legs is performed through getting joints' values in walking state and generating the hip trajectories relative to the foot with forward kinematic model. Inverse kinematic module employs forward kinematic outputs as a trajectory and produces all joint angles according to the particular trajectory input. This verification is straightforward because the calculated joint angles are expected to be the same as the input ones for the forward kinematic module. Complete description of kinematic equations and model validation is available in [20] which comprehensively focused on joint parameters and closed form solution of inverse kinematics.

3.2 Dynamic Model

Position of estimated center of mass which represents the links, drivers and connection effects shall be calculated for the next stages of the dynamic simulation.

Table 2 Joints axes of rotation

Name	Axis	Joint
Roll	X	1,5,8,12
Pitch	Y	2,34,9,10,11
Yaw-Pitch	Y–Z	6,7

This position will be computed from the newly introduced homogenous transformation matrix in Eq. 13

$$T_i = \begin{bmatrix} R_{i,3\times3} & L_{i,3\times1} \\ O_{1\times3} & 1 \end{bmatrix} \tag{13}$$

R_i s are the basic rotation matrix for all 12 joints about three axes and defined in Eq. 14. In addition, L_i s are joints' vectors as shown in Table 3,
Appendix. Basic rotation matrix for three-dimensional transformation in xyz coordinates are as follows:

$$R_{x,\theta} = \begin{bmatrix} 1 & 0 & 0 \\ 0 & \cos\theta & -\sin\theta \\ 0 & \sin\theta & \cos\theta \end{bmatrix}, \quad R_{y,\theta} = \begin{bmatrix} \cos\theta & 0 & \sin\theta \\ 0 & 1 & 0 \\ -\sin\theta & 0 & \cos\theta \end{bmatrix},$$
$$R_{z,\theta} = \begin{bmatrix} \cos\theta & -\sin\theta & 0 \\ \sin\theta & \cos\theta & 0 \\ 0 & 0 & 1 \end{bmatrix} \tag{14}$$

Table 2 represents all 12 joint numbers and their axis of rotation are as depicted in Fig. 1a.

Global position of links' center of mass vectors are defined from the successive multiplication of transformation matrix in Eq. 13 and the local position vectors tabulated in Table 3, Appendix I as:

$$P_{mj} = \left(\prod_{i=1}^{n} T_i \right) L_{mj} \tag{15}$$

$$P_{mi} = \langle x_{mi} \quad y_{mi} \quad z_{mi} \quad 1 \rangle^T \tag{16}$$

where i starts from 1 and ends to the number of joint n before mass i. A dynamic model is developed to determine the joints' angular acceleration for which the mass and diagonal elements of the inertia tensors of each Nao's link are listed in Table 4 and schematically illustrated in Fig. 1b. A movement study of the MRL team Nao robot and ZMP estimation will be done after determination of joint values. The presented dynamic model is for the SSP and will be used as a fundamental calculation for the DSP which is the authors' next research subjects. SSP dynamic equations are derived by the assumption of the Lagrange-d'Alembert Eq. 17 which relates the external force F_i on the Nao links for the single support phase and variations of Lagrangian L relative to the system state r_i.

Table 3 Link vectors and CoM vectors extracted from the Nao physical specifications provided by Aldebaran Co. and geometrical modeling by MRL-Nao team

Center of mass vector (mm)
$L_{m1} = [3.66, -1.52, 38.72]^T$
$L_{m2} = [-3.68, 0.03, 66.79]^T$
$L_{m3} = [-4.80, 50.06, 127.27]^T$
$L_{m4} = [-3.38, -0.03, -33.21]^T$
$L_{m5} = [3.66, 1.52, -64.03]^T$
Joint vector (mm)
$L_1 = [0,0,0]^T$
$L_2 = [0,0,0]^T$
$L_3 = [0,0,102.75]^T$
$L_4 = [0,0,100]^T$
$L_5 = [0,0,0]^T$
$L_6 = [0,0,0]^T$
$L_7 = [0,100,0]^T$
$L_8 = [0,0,0]^T$
$L_9 = [0,0,0]^T$
$L_{10} = [0,0,-100]^T$
$L_{11} = [0,0,-102.75]^T$
$L_{12} = [0,0,0]^T$

Table 4 The mass and diagonal elements of the inertia tensors of each Nao's link

Mass (g)	Inertia (kg × m^2)
$m_1 = 435.98$	$[I_{xx1}, I_{yy1}, I_{zz1}] = [0.0012, 0.0012, 0.0006]$
$m_2 = 605.72$	$[I_{xx2}, I_{yy2}, I_{zz2}] = [0.0018, 0.0018, 0.0010]$
$m_3 = 1026.28$	$[I_{xx3}, I_{yy3}, I_{zz3}] = [0.0049, 0.0047, 0.0016]$
$m_4 = 605.72$	$[I_{xx4}, I_{yy4}, I_{zz4}] = [0.0018, 0.0018, 0.0010]$
$m_6 = 435.98$	$[I_{xx5}, I_{yy5}, I_{zz5}] = [0.0012, 0.0012, 0.0006]$

$$\frac{d}{dt}\left(\frac{\partial L}{\partial \dot{r}_{sn}}\right) - \frac{\partial L}{\partial r_{sn}} = F_n \tag{17}$$

The state vector $\{r_s\}$ consists of the position vectors and the angles as:

$$\{r_s\} = \langle x_1\, y_1\, z_1\, \cdots x_5\, y_5\, z_5\, \theta_1 \cdots \theta_{12} \rangle^T \tag{18}$$

The Lagrangian L is defined as the difference between a system's kinetic energy and potential energy and could be written as follows:

$$L = \sum_{n=1}^{Number\ of\ Links} \frac{1}{2} m_n (\dot{x}_n^2 + \dot{y}_n^2 + \dot{z}_n^2 - 2gz_n) + \frac{1}{2} \vec{\omega}_n^T I_n \vec{\omega}_n \tag{19}$$

In which m_n is the mass of nth link, I_n is the inertia tensor of nth link around base frame, and $\vec{\omega}_n$ is the angular velocity vector of the link n around base frame. j is the total number of link masses which is 5. Partial differentiation of Eq. 19 with regards to $\vec{r}_s$ and $\dot{\vec{r}}_s$ yields:

$$\frac{\partial L}{\partial \vec{r}_s} = \left\langle \frac{\partial L}{\partial x_1} \frac{\partial L}{\partial y_1} \frac{\partial L}{\partial z_1} \cdots \frac{\partial L}{\partial x_5} \frac{\partial L}{\partial y_5} \frac{\partial L}{\partial z_5} \frac{\partial L}{\partial \theta_1} \cdots \frac{\partial L}{\partial \theta_{12}} \right\rangle^T \tag{20}$$

$$\frac{\partial L}{\partial \dot{\vec{r}}_s} = \left\langle \frac{\partial L}{\partial \dot{x}_1} \frac{\partial L}{\partial \dot{y}_1} \frac{\partial L}{\partial \dot{z}_1} \cdots \frac{\partial L}{\partial \dot{x}_5} \frac{\partial L}{\partial \dot{y}_5} \frac{\partial L}{\partial \dot{z}_5} \frac{\partial L}{\partial \dot{\theta}_1} \cdots \frac{\partial L}{\partial \dot{\theta}_{12}} \right\rangle^T \tag{21}$$

Differentiating Eq. 21 results in the determination of the left side of Eq. 17. This vector contains all links' linear and angular accelerations.

The global angular velocities $\vec{\omega}_n$ are calculated in Eq. 22 as described in [23] with consideration of the previous link position and rotation matrix. $\{\zeta\}$ vector represents the axis about which $\dot{\theta}_n$ rotation takes place.

$$\vec{\omega}_n = \vec{\omega}_{n-1} + {}^0_n R\, \dot{\theta}_n \{\zeta\} \tag{22}$$

The torque exerted on the links by electrical drivers could be calculated after mapping the Lagrange-d'Alembert equation to the actuators with implementation of Jacobian as:

$$\{T\} = J_{LJ}(\{\theta\})^T \left(\frac{d}{dt} \left(\frac{\partial L}{\partial \dot{\vec{r}}} \right) - \frac{\partial L}{\partial \vec{r}} \right) \tag{23}$$

In which $J_{LJ}(\{\theta\})$ is the Jacobian for mapping the Lagrange to the joints and mathematically described as:

$$J_{LJ}(\{\theta\}) = \frac{\partial \{r\}}{\partial \{\theta\}} = \begin{bmatrix} \frac{\partial r_{(1,1)}}{\partial \theta_1} & \cdots & \frac{\partial r_{(1,1)}}{\partial \theta_{12}} \\ \vdots & \vdots & \vdots \\ \frac{\partial r_{(27,1)}}{\partial \theta_1} & \cdots & \frac{\partial r_{(27,1)}}{\partial \theta_{12}} \end{bmatrix} \tag{24}$$

The generalized equation of motion of each actuator with consideration of $M(\{\theta\})$ for inertia effect, $C(\{\theta\}, \{\dot{\theta}\})$ for coriolis and centrifugal effects, and $B(\theta)$ for gravitational effect is described in Eq. 25.

$$\{T\} = M(\{\theta\})\{\ddot{\theta}\} + C(\{\theta\}, \{\dot{\theta}\}) + B(\{\theta\}) \tag{25}$$

This yields to determination of $\{\ddot{\theta}\}$ in Eq. 26 with the presence of the total exerted torque vector $\{T\}$ by actuators.

$$\left\{\ddot{\theta}\right\} = M^{-1}(\{\theta\}) \Big(\{T\} - C(\{\theta\}, \{\dot{\theta}\}) - B(\{\theta\}) \Big) \tag{26}$$

Equation 25 requires the predicted joint angles according to the trajectory requirements, but Eq. 26 results in the real joint angles with the robots inertia, coriolis, and centrifugal effects and exerted torques on joints. The main idea of developing control methods on MRL-Nao robots such as torque control or adaptive controllers on joint positions necessitates a comparison between the predefined and feedback joint values.

4 Results and Discussion

The generated trajectory performs as an input for the inverse kinematic model to produce the required joints' angles, velocities and accelerations $\theta_r, \dot{\theta}_r, \ddot{\theta}_r$. The following curves depict joint angles θ_1 to θ_{12} for the predefined trajectory. θ_1 to θ_6 is for the right leg and θ_7 to θ_{12} is contributed to the left leg.

The input torso trajectory could be a cubic type presented in Eqs. 1–5 or real sensory data on the torso and foot provided by experimental results of biped robots. Experimental data of 12 joint angles regarding the Nao trajectory is shown in Figs. 2, 3 and 4. $\theta_5, \theta_6, \theta_7$ and θ_8 symbolize the right leg's hip roll and hip yaw-pitch and left leg's hip yaw-pitch and hip roll angles in Fig. 3 respectively.

Numerical differentiation is employed to determine the joints' angular velocities and accelerations in which time intervals play a significant role. These time intervals are well regulated form the joints sensory position data in this research.

Calculation of joint torques needs joint position specifications as it is stated in Eq. 21 and graphically illustrated in Figs. 5, 6 and 7 in which torque values are shown for all 12 joints.

Drivers' torques are plotted with the supposition of right leg as the supporting leg on the ground and left leg as the non-supporting leg.

Assumption of left leg as the non-supporting leg justifies small values of calculated T_9 and T_{10} values in comparison with the corresponding joints on the right leg and zero values for T_{11} and T_{12}.

Phase estimator calculates the phase parameters for SSP and DSP states, and then joints' reference angles are used in the forward kinematic model together with the phase estimator to produce all links' state position, velocity and acceleration vectors $\{r_s\}, \{\dot{r}_s\}, \{\ddot{r}_s\}$.

Generalized position vectors of links and five masses shown in Fig. 1b are estimated by Eq. 15, then velocity and acceleration values are achievable with numerical differentiation. Figures 8 and 9 demonstrate acceleration of two assumed mass on the torso and the right leg shown as m_2 and m_3 in Fig. 1b.

State position vectors and actuator torques are executed in the dynamic model to generate real joints' angles and velocities. The reference joint angles are compared with the estimated ones to build up a reliable controller such as adaptive PID or fuzzy logic controller. Torque control is this group's next research topic in order to reach a smooth Nao bipedal motion on the slopes.

All plotted curves are based on single support assumption of the right leg, but the transient mode and successive leg changes have not been considered in this simulation. Torque increase at specified times shows this change and may result into some errors in the calculated joint torques.

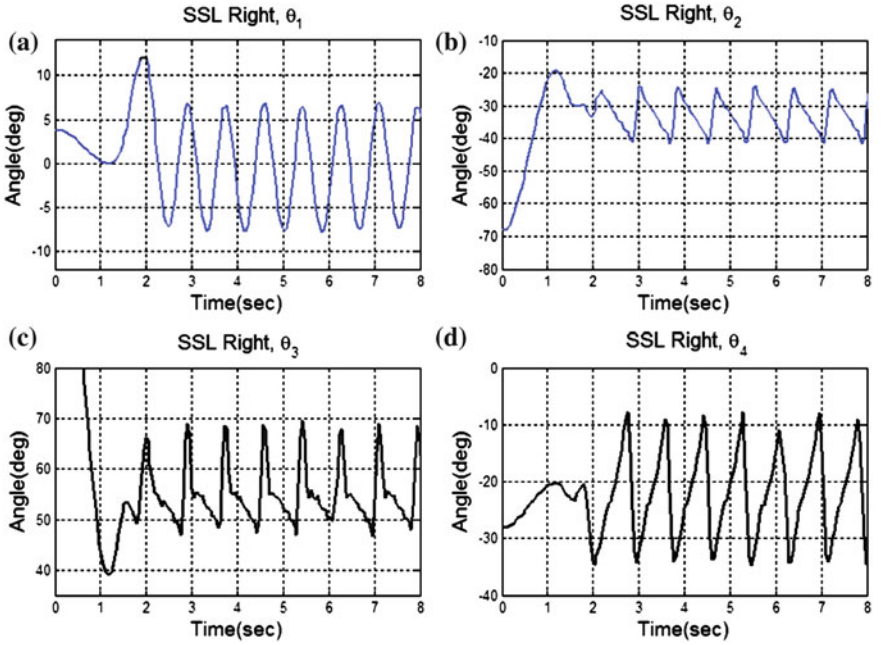

Fig. 2 **a** ankle roll, **b** ankle pitch, **c** knee pitch, and **d** hip pitch joint angles on the right leg extracted from real sensory data

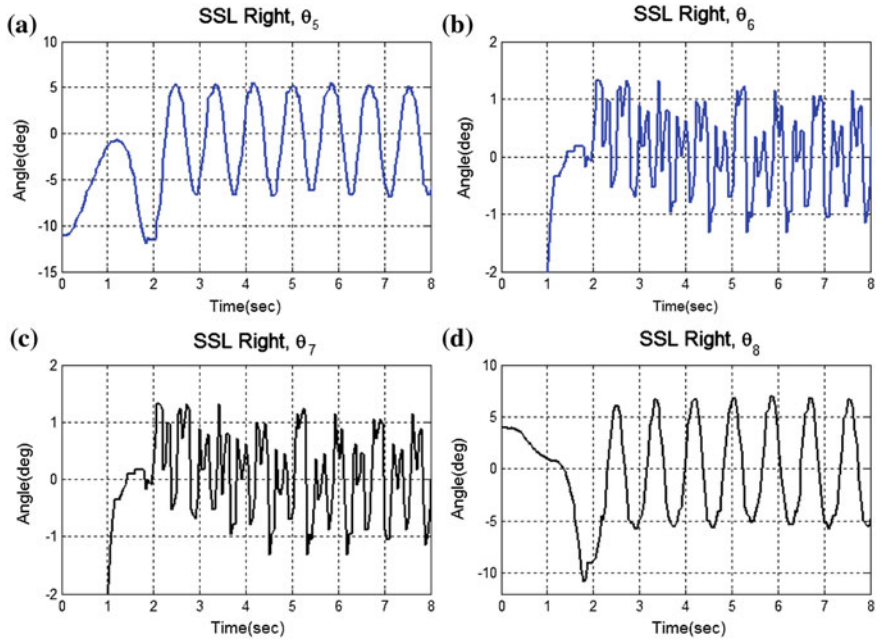

Fig. 3 Real sensory data of (**a**) right hip roll, (**b**) right hip yaw-pitch, (**c**) left hip yaw-pitch, (**d**) left hip roll

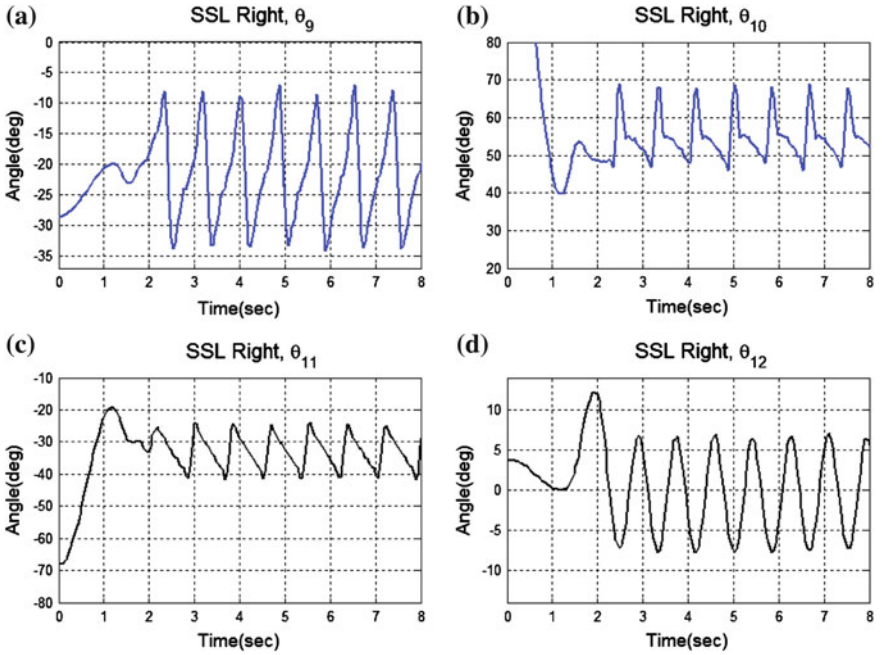

Fig. 4 **a** Hip pitch, **b** knee pitch, **c** ankle pitch, and **d** ankle roll joints angles on the left leg extracted from real sensory data

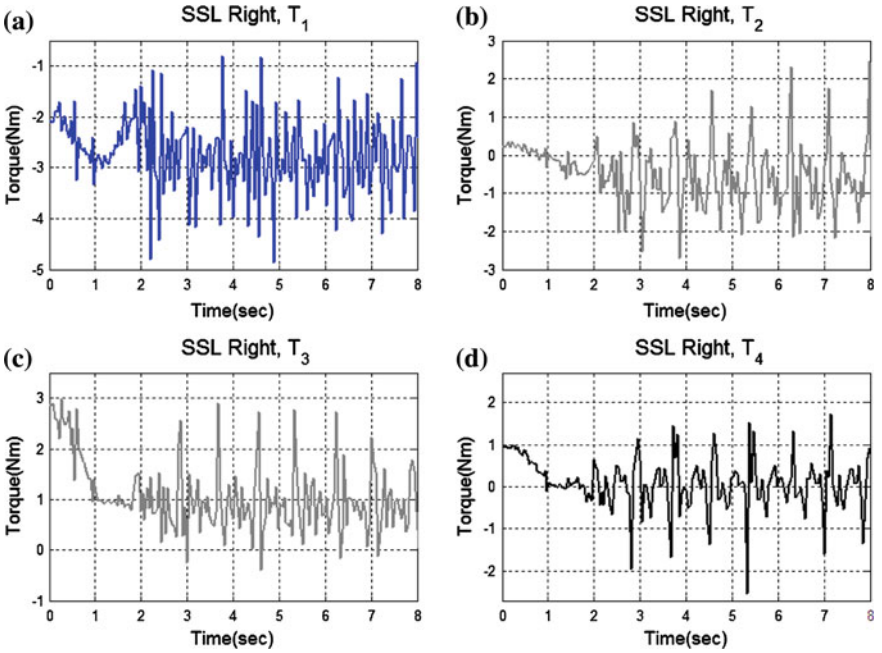

Fig. 5 Driver torques calculated by desired trajectories for (**a**) ankle roll, (**b**) ankle pitch, (**c**) knee pitch, and (**d**) hip pitch joints on the right leg

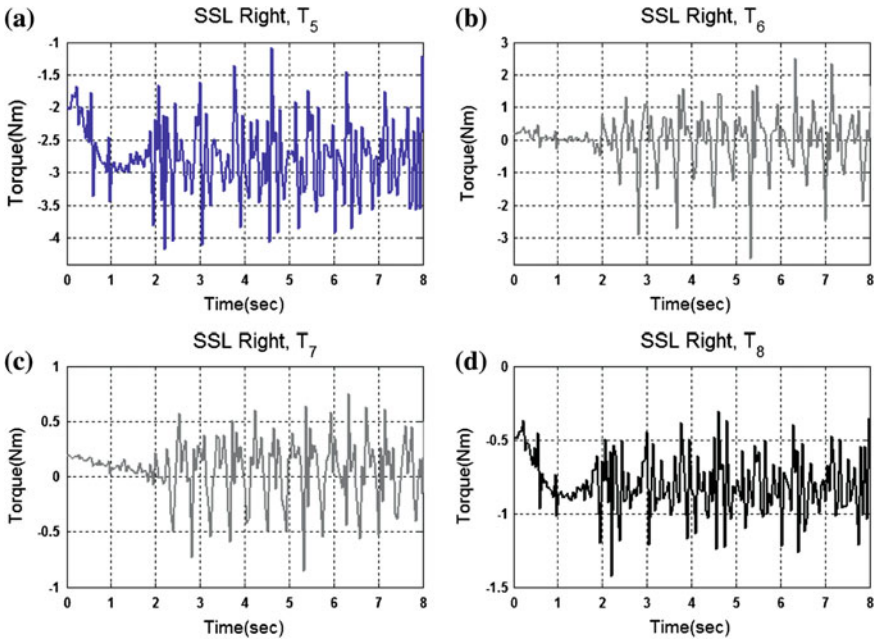

Fig. 6 Driver torques calculated by desired trajectories for (**a**) right hip roll, (**b**) right hip yaw-pitch, (**c**) left hip yaw-pitch, (**d**) left hip roll joints

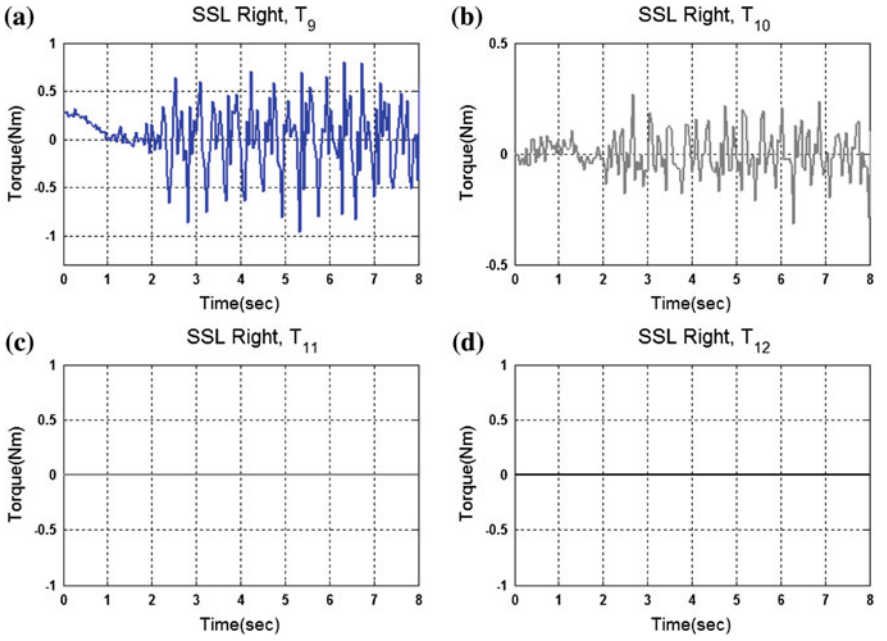

Fig. 7 Driver torques estimated by desired trajectories for (**a**) hip pitch, (**b**) knee pitch, (**c**) ankle pitch, and (**d**) ankle roll joints of the left leg

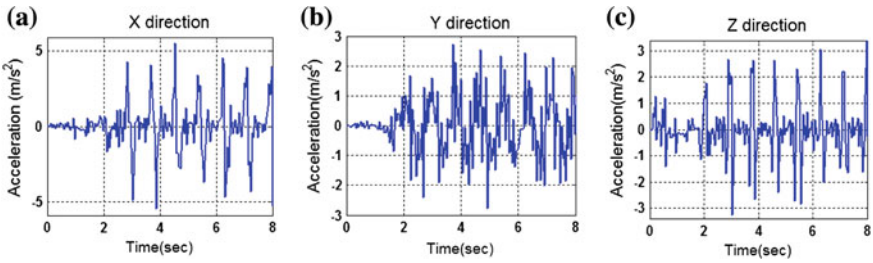

Fig. 8 Acceleration of mass 2 on the right leg computed by generalized position vector

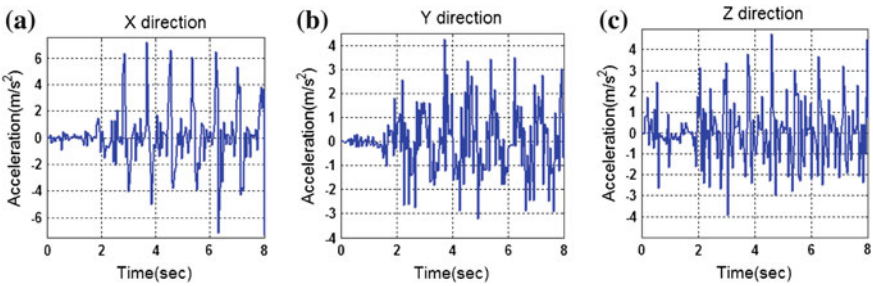

Fig. 9 Acceleration of dedicated mass on torso, m^3, obtained by generalized position vector

5 Conclusions

The proposed dynamic model and related analysis in this chapter simulates the joint values including torque and angular acceleration for the recorded trajectories as the real sensory data. The observed fluctuations on the torque curves are produced during the change support leg behavior in which acceleration values of joint oscillate due to transient phase between SSP and DSP.

The proposed transformation matrix in Eq. 13 contains rotation and position vectors of the joints and reduces the total number of calculation as a combined transformation.

Optimization in trajectories and parameters regulation could improve performance of the robot and lead to minimum energy consumption. Authors' future research topics are focused on a) torso trajectory optimization by genetic algorithm and particle swarm optimization, b) adding the double support phase and the transient mode, and c) torque control for performing stable walk on slopes.

Acknowledgments Authors gratefully acknowledge Qazvin Islamic Azad University, Young Researchers Club (YRC), and technical support of Mechatronics Research Lab. Nao team members.

6 Appendix

Position constraints of foot and torso in *sagittal* plane are defined as:

$$x_f(t) = \begin{cases} (k-1)L_{step} & ,t = t_1 \\ (k-1)L_{step} & ,t = t_2 \\ (k-1)L_{step} + L_{\max} & ,t = t_3 \\ (k+1)L_{step} & ,t = t_4 \end{cases} \quad z_f(t) = \begin{cases} FootHeight & t = t_1 \\ FootHeight & t = t_2 \\ h_{f\max} & t = t_3 \\ FootHeight & t = t_4 \end{cases} \tag{A.1}$$

In which L_{step} is the step length, $L_{\max}$ is the maximum horizontal distance of the ankle from the start point in $T_{\max}$, $h_{f\max}$ is the maximum ankle height during T_{step}. Constraints in torso position for specified times are as below:

$$x_t(t) = \begin{cases} kL_{step} - 1.3x_{ts} & ,t = t_1 \\ kL_{step} - x_{ts} & ,t = t_2 \\ kL_{step} + x_{te} & ,t = t_4 \end{cases}, y_t = \begin{cases} y_{tmid} & ,t = t_1 \\ y_{t\min} & ,t = t_3 \end{cases}, z_t(t) = \begin{cases} h_{t\min} & ,t = t_1 \\ h_{t\max} & ,t = t_3 \\ h_{t\min} & ,t = t_4 \end{cases} \tag{A.2}$$

y_{tmid} stands for the distance between the feet and $y_{t\min}$ is the minimum distance from the ankle of the supporting foot to the spinal column. Experimental results substantiate the margin of $y_{t\min}$ between $-0.2\,y_{tmid}$ and $0.4\,y_{tmid}$. Furthermore, $h_{t\max}$ and $h_{t\min}$ symbolizes maximum and minimum torso height (Tables 3, 4.

Approximation functions of Eq. 9 in text are described as:

$$f_1(\theta_3) = a_3(c\theta_3) + d_4 s\alpha_3(s\theta_3) + a_2 \tag{A.3}$$

$$f_2(\theta_3) = a_3 c\alpha_2(s\theta_3) - d_4 s\alpha_3 c\alpha_2(c\theta_3) - d_4 s\alpha_2 c\alpha_3 - d_3 s\alpha_2 \tag{A.4}$$

$$f_3(\theta_3) = a_3 s\alpha_2(s\theta_3) - d_4 s\alpha_3 s\alpha_2(c\theta_3) + d_4 c\alpha_2 c\alpha_3 + d_3 c\alpha_2 \tag{A.5}$$

$$g_1(\theta_2, \theta_3) = [c\theta_2 f_1(\theta_3)] - [s\theta_2 f_2(\theta_3)] + a_1 \tag{A.6}$$

$$g_2(\theta_2, \theta_3) = c\alpha_1[s\theta_2 f_1(\theta_3)] + c\alpha_1[c\theta_2 f_2(\theta_3)] - s\alpha_1[f_3(\theta_3)] - d_2 s\alpha_1 \tag{A.7}$$

$$g_3(\theta_2, \theta_3) = s\alpha_1[s\theta_2 f_1(\theta_3)] + s\alpha_1[c\theta_2 f_2(\theta_3)] + c\alpha_1[f_3(\theta_3)] + d_2 c\alpha_1 \tag{A.8}$$

References

1. Goswami, A. Kinematic and dynamic analogies between planar biped robots and the reaction mass pendulum (RMP) model. In: Proceedings of the 8th IEEE-RAS International Conference on Humanoid Robots, pp. 182–188 (2008)
2. Kagami, S., Mochimaru, M., Ehara, Y., Miyata, N., Nishiwaki, K., Kanade, T., Inoue, H.: Measurement and comparison of humanoid H7 walking with human being. J. Robot. Auton. Syst. **48**, 177–187 (2003)

3. Wollherr, D., Buss, M., Hardt, M., Stryk, O.V.: Research and development towards an autonomous biped walking robot. In: Proceedings of the IEEE/ASME International Conference on Advanced Intelligent Mechatronics, AIM (2003)
4. Fujimoto, Y.:Trajectory generation of biped running robot with minimum energy consumption. In: Proceedings of the IEEE International Conference on Robotics & Automation, pp. 3803–3808 (2004)
5. Huang, O., Yokoi, K., Kajita, S., Kaneko, K., Arai, H., Koyachi, N., Tanie, K.: Planning walking patterns for a biped robot. IEEE Trans. Robot. Autom. **17**, 280–289 (2001)
6. Sugihara, T., Nakamura, Y., Inoue, H.: Real time humanoid motion generation through ZMP manipulation based on inverted pendulum control. In: The Proceedings of the IEEE International Conference on Robotics & Automation, pp. 1404–1409 (2002)
7. McGee, T.G., Spong, M.W.: Trajectory planning and control of a novel walking biped. IEEE Conf. Control Appl, 1099–1104 (2001)
8. Kajita, S., Morisawa, M., Harada, K., Kaneko, K., Kanehiro, F., Fujiwara, K., Hirukawa, H.:Biped walking pattern generator allowing auxiliary ZMP control. In: Proceedings of the IEEE/RSJ International Conference on Intelligent Robots and Systems, pp. 2993–2999 (2006)
9. Kajita, S., Kanehiro, F., Kaneko, K., Fujiwara, K., Harada, K., Yokoi, K., Hirukawa, H.:Biped walking pattern generation by using preview control of zero-moment point. In: Proceedings of the IEEE International Conference on Robotics and Automation (2003)
10. Hurmuzlua, Y., Genot, F., Brogliatoc, B.: Modeling, stability and control of biped robots-a general framework. Automatica **40**, 1647–1664 (2004)
11. Colbaugh, R., Glass, K., Seraji, H.: An adaptive inverse kinematics algorithm for robot manipulators. Int. J. Model. Simul **11**(2), 33–38 (1991)
12. Azevedo, C., Andreff, N., Arias, S.: Bipedal walking: from gait design to experimental analysis. Mechatron Elsevier **14**(6), 639–665 (2004)
13. Wieber, P. B.: Trajectory free linear model predictive control for stable walking in the presence of strong perturbations. In: Proceedings of the IEEE International Conference on Humanoids, pp. 137–142 (2006)
14. Vukobratović, M., Borovac, B., otkonjak, V. :Contribution to the synthesis of biped gait. In: Proceedings of the IFAC Symposium on Technical and Biological Problem and Control (1969)
15. Huang, Q., Yokoi, K., Kajita, S., Kaneko, K., Arai, H., Koyachi, N., Tanie, K.: Planning walking patterns for a biped robot. IEEE Trans Robot Autom **17**(3), 874–879 (2001). June
16. Choi, Y., You, B. J., Oh, S. R.: On the stability of indirect ZMP controller for biped robot systems. In: Proceedings of International Conference on Intelligent Robots and Systems, 1966–1971 (2004)
17. Huang, Q., Kaneko, K., Yokoi, K., Kajita, S., Kotoku, T., Koyachi, N., Arai, H., Imamura, N., Komoriya, K., Tanie, K.: Balance control of a biped robot combining off-line pattern with real-time modification. In: Proceedings of the 2000 IEEE International Conference on Robotics and Automation San Francisco, pp. 3346–3352, April 2000
18. Huang, O., Kajita, S., Koyachi, N., Kaneko, K., Yokoi, K., Arai, H., Komoriya, K., ane, K.: A high stability, smooth walking pattern for a biped robot. In: Proceedings of the IEEE International Conference on Robotics and Automation, pp. 65–71 (1999)
19. Jensen, B.T., Niss M.O.: Modeling, simulation, and control of biped robot AAU-BOT1. Master's thesis, Aalborg University (2009)
20. Ghaffari Jadidi, M., Hashemi, E., Zakeri Harandi, M.A., Sadjadian, H.: Kinematic Modeling Improvement and Trajectory Planning of the Nao Biped Robot. In proceedings of the Joint International Conference on Multibody System Dynamics, Finland, May 2010
21. Zannatha, J.I., Limon, R.C.: Forward and inverse kinematics for a small-sized humanoid robot. In: Proceedings of the 19th IEEE International Conference on Electrical. Communications and Computers, pp. 111–118 (2009)
22. Christensen, J., Nielsen, J.L., Svendsen, M.S., Ørts, P.F.: Development, modeling and control of a humanoid robot, Master's thesis, Aalborg University (2007)

23. John, J.: Craig, Introduction to Robotics: Mechanics and Control, Pearson Prentice Hall, 3rd edn (2005). ISBN: 0-13-123629-6
24. Mu, X., Wu, Q.: A complete dynamic model of five-link bipedal walking. Proc. Am. Control Conf. **6**, 4926–4931 (2003)
25. Goldenberg, A.A., Benhabib, B., Fenton, R.G.: A complete generalized solution to the inverse kinematics of robots. IEEE J. Robot. Autom. (RA) **1**(1), 14–20 (1985)